Built-in Electric Field Triggered Interfacial Electron Accumulation and Structural Reconstruction for Boosting Ampere-Level-Current Seawater Oxidation

Supplementary information

List of contents

1. Experimental Section

1.1 Materials

Nickel sulfate heptahydrate ($NiSO_4 \cdot 7H_2O$, AR, 98.0%), Nickel nitrate hexahydrate ($Ni(NO_{3)2} \cdot 6H_2O$, AR, 98.0%), Ferric nitrate nonahydrate ($Fe(NO_3)_3 \cdot 9H_2O$, AR, 98.5%), acetone (C_3H_6O, 99.5%), ethanol (C_2H_6O, 99.5%), potassium hydroxide (KOH, 85%), were purchased from Sinopharm Chemical Reagent Co., LTD. Commercial iridium dioxide (IrO_2， 99.9%), and Nafion (5 wt%) were purchased from Shanghai Aladdin Biochemical Technology Co., Ltd. The deionized (DI) water used in the solution preparation and washing steps comes from ultrapure water (Milli-Q, 18 MΩ·cm) made in the laboratory. Iron-nickel foam (FNF, 1.0 mm, porosity: 110 ppi) was obtained from Kunshan Xingzhenghong Electronic Materials Co., LTD. were used as the substrate. All chemicals were analytical grade and used as received without further purification.

1.2 Treatment of iron-nickel foam

In order to remove the surface oxide layer, a piece of iron-nickel foam (FNF) (1×4 cm^2) was treated in acetone under ultrasonication for 0.5 h, followed by sonicating several times with ethanol and DI water successively, and finally dried in a vacuum oven at 60 °C for 6 h.

1.3 Fabrication of $Fe(OH)_3$/FNF electrode

For comparative study, $Fe(OH)_3$/FNF was prepared based on the literature method as follow:[1] 1.414 g (3.5 mmol) $Fe(NO_3)_3 \cdot 9H_2O$ was dissolved in 50 mL ethanol. The FNF substrate was immersed in the solution for a duration of 12 h. Subsequently, the FNF was then rinsed extensively several times using deionized water and ethanol, then dried in a vacuum oven (60 °C, 6h).

1.4 Fabrication of IrO_2/FNF electrode

2.1 mg of IrO_2 powder was dispersed in a mixed solution containing ethanol (1 mL) and Nafion binder (5 wt%, 55 μL) through ultrasonication to form a homogeneous ink dispersion. The resulting dispersion was uniformly coated onto a pre-treated FNF substrate (1 × 1 cm^2), followed drying at 60 °C for 2 h in room.

1.5 Fabrication of $Ni(OH)_2$/FNF electrode

The $Ni(OH)_2$/FNF was prepared as the literature[2] by electrodeposited method on

FNF. A solution of 0.1 M of $Ni(NO_3)_2$ was used for the electrodeposition. The two-electrode configuration with Pt coil as the reference and FNF (1 cm×1 cm) as the working electrode. The electrodeposition was carried out at 1.5 mA cm^2 for 160 s. After plating, the electrode was cleaned with deionized water.

1.6 General characterizations

The microstructure and phase information of catalysts using X-ray diffraction (XRD, Rigaku Ultima IV, Cu Kα, λ = 1.54056 Å), field-emission scanning electron microscope (FESEM, JSM-7610F, 15 kV), and Transmission electron microscopy (TEM, JEOL 2010F) with EDS. The surface characteristics were investigated using X-ray photoelectron spectroscopy (XPS, Thermo Fisher Scientific K-Alpha, Mg Kα. Ultraviolet photoelectron spectroscopy (UPS) is performed on Thermo ESCALAB Xi+ equipped with ultraviolet photoelectron spectrometer (Hel (21.22 eV)). In-situ Raman spectroscopy measurements were conducted using a confocal micro-Raman spectrometer (Renishaw inVia) coupled with an electrochemical workstation. The contact angle data of liquid and bubbles were measured using a JY-82B instrument.

1.7 Electrochemical test

Electrochemical measurements were conducted using a PARSTAT (P4000) workstation with a three-electrode configuration: Hg/HgO as the reference, graphite as the counter, and prepared samples as the working electrode.

The prepared samples, graphite rod, and a Hg/HgO electrode were used as working, counter, and reference electrode, respectively. The electrolytes is natural alkaline seawater (1 M KOH+SW). Natural seawater was collected from the Bohai bay in China, Qinhuangdao, Shandong, China. The collected natural seawater is firstly filtered by a 0.22 μm filtration membrane, then added KOH, and finally centrifuged to remove sediment and use as seawater electrolyte.

The potentials were converted to the reversible hydrogen electrode (RHE) by the equation: $E_{RHE} = E_{Hg/HgO} + 0.098 + 0.0591 \times pH$. The catalytic performances of samples were evaluated using LSV at 5 mV s^{-1}. The LSV curves were calibrated using a 70% solution resistance correction.

All the LSV curves were derived from multiple tests to ensure data consistency. Electrochemical impedance spectroscopy (EIS) was conducted across a frequency from 10^5 to 10^{-2} Hz with 5 mV AC amplitude.

The Tafel slope was calculated according to Equation: $\eta = \alpha + \frac{2.3RT}{\alpha nF} log|j|$, where η is the overpotential, j is the current density, α is the transfer coefficient, n is the number of electrons involved in the reaction, F is the Faradaic constant, b = 2.3RTαnF is the value of Tafel slope.

A two-electrode overall seawater splitting (OSWS) electrolyzer equipped with FNF as cathode and Ni-Fe(OH)$_3$/FNF anode was constructed. The Faraday efficiency of the electrolyzer is calculated based on the ratio of the volume of collected ($V_{collected}$) H_2/O_2 evolved to the calculated one ($V_{calculated}$):

$$\text{Faraday efficiency} = \frac{Vcollected}{V_{calculated}} \times 100\%$$

The actual volumes of generated H_2/O_2 gas were gathered using the drainage method at constant 1.7 V with a current density of 50 mA cm^{-2}. The theoretical volume can be calculated by the formula:

$$V_{calculated} = \frac{I \cdot t \cdot V_m}{n \cdot F}$$

where I is current density (A), t is time (s), V_m is molar volume of H_2/O_2 gas (22.4 L mol^{-1}, in Hanzhong, Shaanxi), F is the Faraday constant (96485 C mol^{-1}), *n* is electron number transferred per molecule (n is 2 and 4 for HER and OER, respectively).

1.8 DFT calculation details

All the calculations were performed within the framework of density functional theory (DFT) using the projector augmented plane-wave method, as implemented in the Vienna ab initio simulation package (VASP).[3, 4] The generalized gradient approximation proposed by Perdew-Burke-Ernzerhof was selected for the calculation of exchange-correlation potentials. [5]The cutoff energy for plane waves was set to 400 eV. The energy criterion was set to be 10^{-5} eV for obtaining the iterative solution of the

Kohn-Sham equation. A 3 × 3 × 1 k-mesh was used for the structural optimizations of Ni-FeOOH, FeOOH.

A 15 Å vacuum region was set in the z-direction to prevent interactions between two adjacent surfaces. The force and convergence thresholds for energy were less than 0.02 eV $Å^{-1}$ and 10^{-5} eV, respectively. During the calculations, the bottom layers of the structures were fixed. The reaction Gibbs free energy (ΔG) of the intermediates was determined using $\Delta G = \Delta E + \Delta ZPE - T\Delta S$, where T is the temperature (298.15 K), ΔZPE is zero-point energy, ΔE is the reaction energy, and ΔS is the entropy difference calculated from the vibration frequency. The entropies of H_2O vapor under standard conditions were obtained from the NIST database. The computational conditions employed to construct the OER configuration are 0 V vs. NHE.

2. Supplementary figures

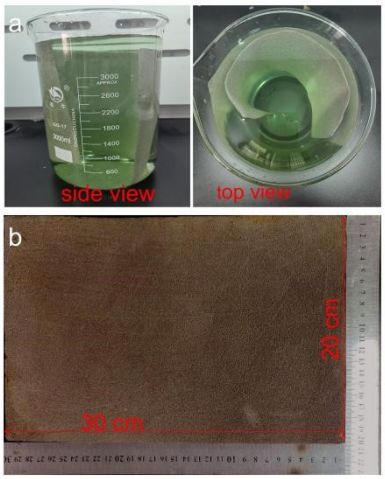

Figure S1. Diagram of the preparation process of large-scale electrode, (a) side and top view, (b) photograph of Ni-$Fe(OH)_3$/FNF.

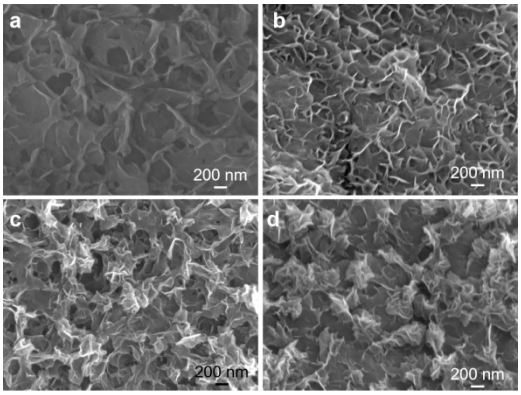

Figure S2. SEM images of Ni-Fe(OH)$_3$/FNF-n, (a) 4h, (b) 8h, (c)12h, and (d) 16h.

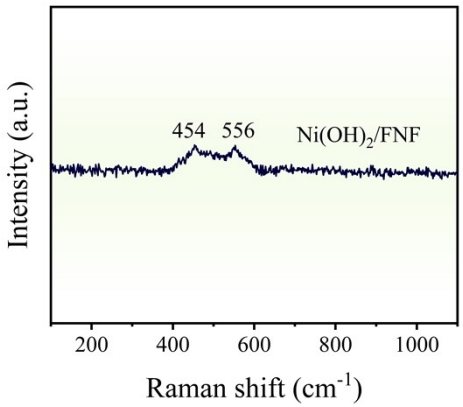

Figure S3. Raman spectrum of Ni(OH)$_2$/FNF

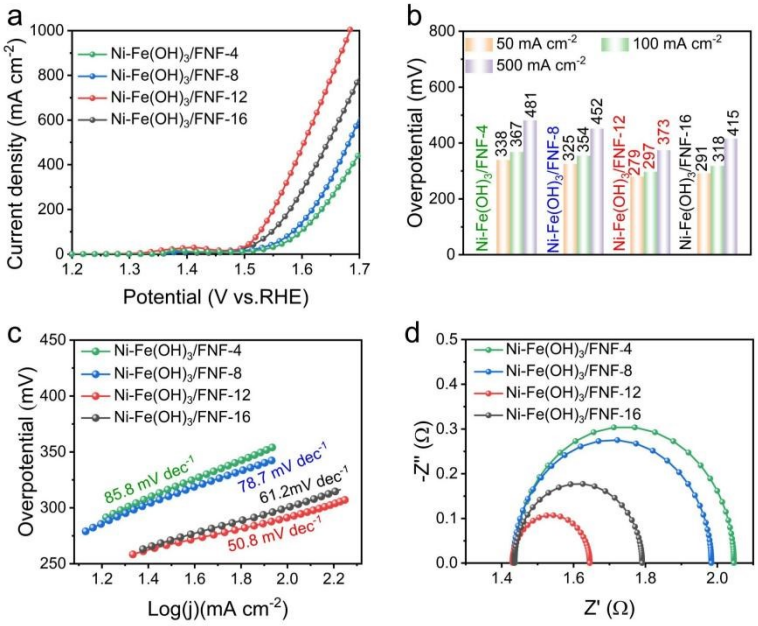

Figure S4. OER performance of Ni-Fe(OH)$_3$/FNF-n (n=4, 8, 12, and 16 h).

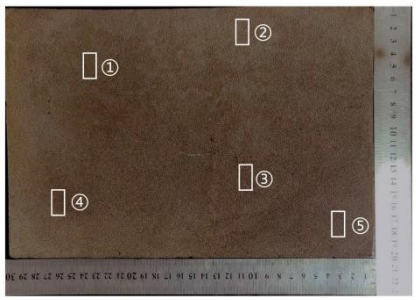

Figure S5. Different region of Ni-Fe(OH)$_3$/FNF-12.

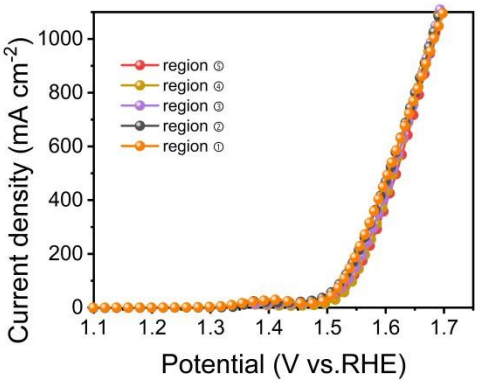

Figure S6. LSV curves of different region of Ni-Fe(OH)$_3$/FNF-12.

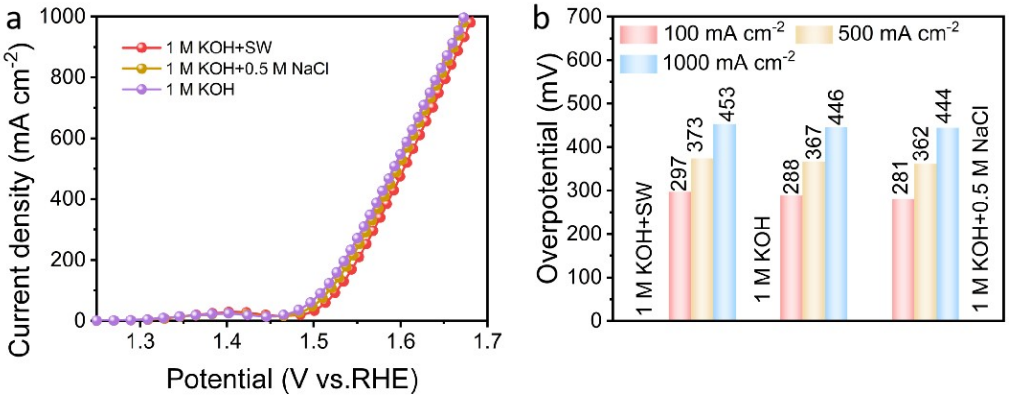

Figure S7. OER performance of Ni-Fe(OH)$_3$/FNF in different electrolyte. (a) LSV, (b) overpotential.

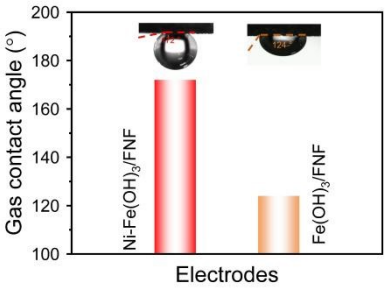

Figure S8. Gas contact angle of electrodes.

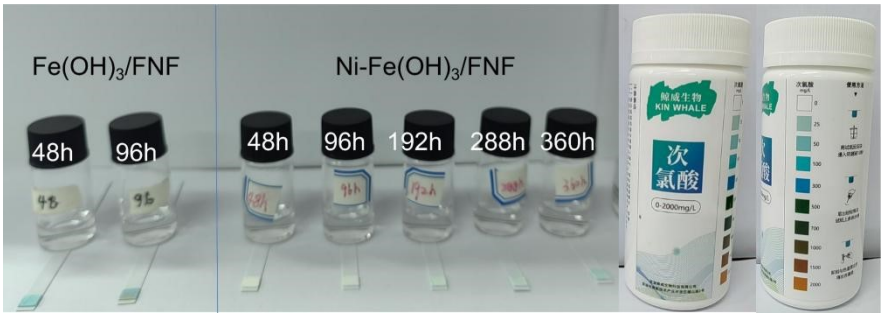

Figure S9. Methods for detecting ClO^- by the ClO-indicator.

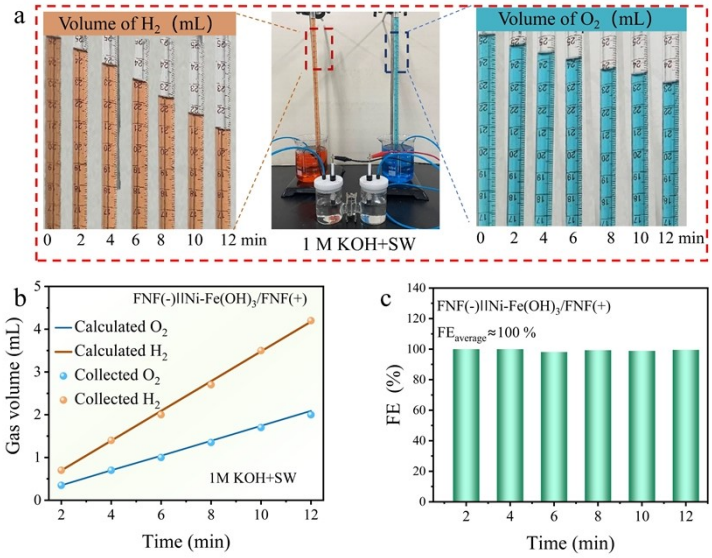

Figure S10. Drainage method for Faraday efficiency test: (a) Picture of OWSW drainage test, (b) Gas production with different duration time, (c) Calculated Faraday efficiency.

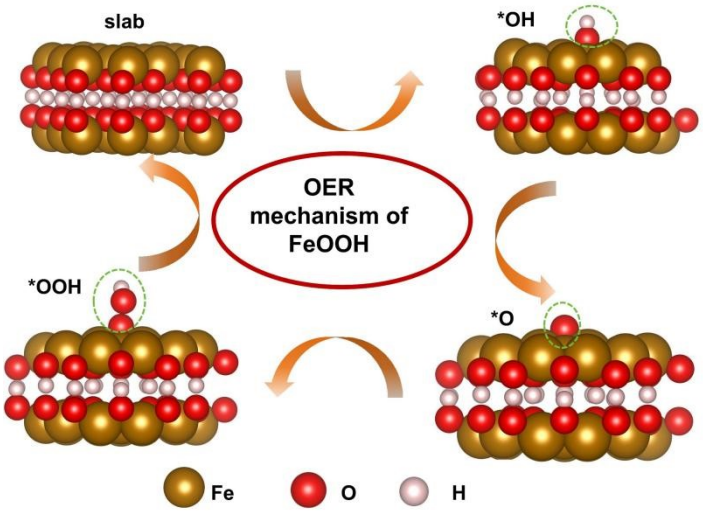

Figure S11. OER mechanism of FeOOH at Fe sites.

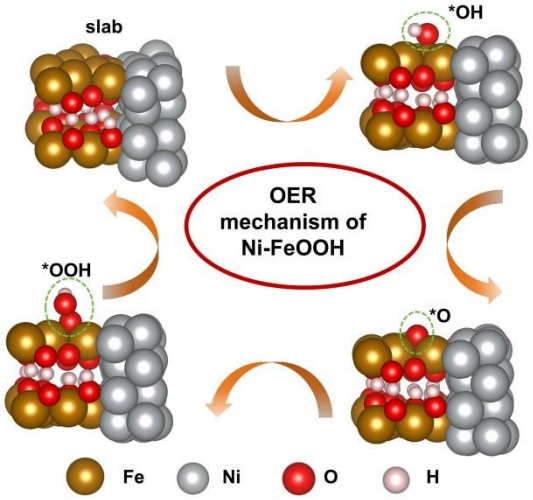

Figure S12. OER mechanism of Ni-FeOOH at Fe sites.

Table S1 The XPS peak parameters of Ni-$Fe(OH)_3$ and $Fe(OH)_3$

	Ni-$Fe(OH)_3$			$Fe(OH)_3$		
	BE (eV)	FWHM (eV)	assignment	BE (eV)	FWHM (eV)	assignment
Ni $2p_{1/2}$	852.7	1.5	Ni(0)	–	–	–
Ni $2p_{3/2}$	869.9	0.9	Ni(0)	–	–	–
Fe$2p_{1/2}$	722.4	2.0	Fe (II)	722.5	2.0	Fe (II)
Fe$2p_{1/2}$	724.4	2.5	Fe (III)	724.5	2.5	Fe (III)
Fe $2p_{3/2}$	709.4	2.0	Fe (II)	709.8	2.0	Fe (II)

Fe $2p_{3/2}$	711.1	2.5	Fe (III)	711.4	2.5	Fe (III)
O 1s	529.5	1.5	O-H	529.5	1.5	O-H
O 1s	531.1	1.6	O-M	531.0	1.6	O-M
O 1s	532.5	2.1	H_2O	532.4	2.1	H_2O

Table S2 Overpotentials comparison at 500 mA cm^{-2} for Ni-$Fe(OH)_3$/FNF with reported electrocatalysts in 1 M KOH + seawater.

Electrocatalysts	η (mV)	References
Ni-$Fe(OH)_3$/FNF	373	This work
Fe-$Ni(OH)_2$/Ni_3S_2@NF	390	[6]
Pt-CoFe(Ⅱ) LDH	375	[7]
(FeOOH/FeNiCo-LDH/HCNC	377	[8]
NH_2–CoFe MOF	428	[9]
Fe-CoCH/NF	387	[10]
Ni_3FeN@C/NF	394	[11]
S-FeOOH/NiOOH	370	[12]
S-Ni/Fe(OOH)/NF	398	[13]
Fe-NiS/NF	420	[14]

Reference

[1] S. Hao, Y. Wei, X. Chen, M. Cong, X. Ding, Y. Gao, Amorphous $Fe(OH)_3$ electro-deposited on 3D cubic $MnCO_3$ for enhanced oxygen evolution, Int. J. Hydrogen Energy, 47 (2022) 17263-17270, https://doi.org/10.1016/j.ijhydene.2022.03.200.

[2] S.-Y. Lee, I.-S. Kim, H.-S. Cho, C.-H. Kim, Y.-K. Lee, Resolving potential-dependent degradation of electrodeposited $Ni(OH)_2$ catalysts in alkaline oxygen evolution reaction (OER): In situ XANES studies, Appl. Catal. B Environ., 284 (2021) 119729, https://doi.org/10.1016/j.apcatb.2020.119729.

[3] G. Kresse, J. Hafner, Ab initio molecular dynamics for liquid metals, Physical Review B, 47 (1993) 558-561, https://doi.org/10.1103/PhysRevB.47.558.

[4] G. Kresse, D. Joubert, From ultrasoft pseudopotentials to the projector augmented-wave method, Physical Review B, 59 (1999) 1758-1775, https://org.doi/10.1103/PhysRevB.59.1758.

[5] J.P. Perdew, K. Burke, M. Ernzerhof, Generalized gradient approximation made simple, Physical Review Letters, 77 (1996) 3865-3868, https://doi.org/10.1103/PhysRevLett.77.3865.

[6] B. Cui, Z. Hu, C. Liu, S. Liu, F. Chen, S. Hu, J. Zhang, W. Zhou, Y. Deng, Z. Qin, Z. Wu, Y. Chen, L. Cui, W. Hu, Heterogeneous lamellar-edged Fe-$Ni(OH)_2$/Ni_3S_2 nanoarray for efficient and stable

seawater oxidation, Nano Res., 14 (2021) 1149-1155, https://doi.org/10.1007/s12274-020-3164-3.
[7] J. Wu, Z. Nie, R. Xie, X. Hu, Y. Yu, N. Yang, Self-assembled Pt–CoFe layered double hydroxides for efficient alkaline water/seawater splitting by spontaneous redox synthesis, Journal of Power Sources, 532 (2022) 231353, https://doi.org/10.1016/j.jpowsour.2022.231353.
[8] Y. Luo, Y. Yang, Y. Tian, Q. Wu, W.-F. Lin, M. Wen, Collaborative reconstruction of FeOOH/FeNiCo-LDH heterogeneous nanosheets for enhancing anion exchange membrane seawater electrolysis, J. Mater. Chem. A, 13 (2025) 7136-7148, http://doi.org/10.1039/D4TA08586H.
[9] D.H. Kim, J. Moon, S.Y. Lee, H.J. An, H. Jeong, J.T. Park, Fe-modulated NH_2-CoFe MOF nanosheet arrays on nickel foam by cation exchange reaction for an efficient OER electrocatalyst at high current density in alkaline water/seawater, CrystEngComm, 25 (2023) 5387-5398, http://doi.org/10.1039/D3CE00728F.
[10] S. Shi, S. Sun, X. He, L. Zhang, H. Zhang, K. Dong, Z. Cai, D. Zheng, Y. Sun, Y. Luo, Q. Liu, B. Ying, B. Tang, X. Sun, W. Hu, Improved electrochemical alkaline seawater oxidation over cobalt carbonate hydroxide nanowire array by iron doping, Inorg. Chem., 62 (2023) 11746-11750, https://doi.org/10.1021/acs.inorgchem.3c01473.
[11] B. Wang, M. Lu, D. Chen, Q. Zhang, W. Wang, Y. Kang, Z. Fang, G. Pang, S. Feng, Ni_xFe_yN@C microsheet arrays on Ni foam as an efficient and durable electrocatalyst for electrolytic splitting of alkaline seawater, J. Mater. Chem. A, 9 (2021) 13562-13569, http://doi.org/10.1039/D1TA01292D.
[12] X. Sun, Z. Xu, Q. Shi, X. Ma, S. Lin, Sulfur-doped FeOOH/NiOOH electrocatalyst with enhanced activity and stability for ampere-level seawater oxidation, Electrochim. Acta, 536 (2025) 146770, https://doi.org/10.1016/j.electacta.2025.146770.
[13] J. Liu, J. Yang, Y. Song, J. Sun, Y. Tian, Q. Chen, X. Zhang, L. Zhang, Introducing non-bridging ligand in metal-organic framework-based electrocatalyst enabling reinforced oxygen evolution in seawater, J. Colloid Interface Sci., 643 (2023) 17-25, https://doi.org/10.1016/j.jcis.2023.04.009.
[14] C. Yang, K. Dong, L. Zhang, X. He, J. Chen, S. Sun, M. Yue, H. Zhang, M. Zhang, D. Zheng, Y. Luo, B. Ying, Q. Liu, A.M. Asiri, M.S. Hamdy, X. Sun, Improved alkaline seawater splitting of NiS nanosheets by iron doping, Inorg. Chem., 62 (2023) 7976-7981, https://doi.org/10.1021/acs.inorgchem.3c00836.